Available online at www.sciencedirect.com
ScienceDirect
International Journal of Heat and Mass Transfer 50 (2007) 45–57
International Journal of HEAT and MASS TRANSFER
www.elsevier.com/locate/ijhmt

Estimation of heat transfer coefficient on the vertical plate fin of finned-tube heat exchangers for various air speeds and fin spacings

Han-Taw Chen *, Juei-Che Chou, Hung-Chih Wang

Department of Mechanical Engineering, National Cheng Kung University, Tainan 701, Taiwan

Received 20 April 2006
Available online 20 September 2006

Abstract

The finite difference method in conjunction with the least-squares scheme and experimental temperature data is proposed to predict the average heat transfer coefficient $\bar{h}$ and fin efficiency η_f on a vertical square fin of one-circular tube plate finned-tube heat exchangers for various air speeds and fin spacings. The distribution of the heat transfer coefficient on the fin can be very non-uniform, thus the whole square fin is divided into several sub-fin regions in order to predict the $\bar{h}$ and η_f values. These two predicted values can be obtained using the present inverse scheme in conjunction with the knowledge of the temperatures recordings at several selected measurement locations. The results show that the heat transfer coefficient on the upstream fin region can be markedly higher than that on the downstream fin region. The $\bar{h}$ value increases with increasing the fin spacing S and air speed V_{air}, and the η_f value decreases with increasing the S and V_{air} values. The $\bar{h}$ and η_f values respectively approach their corresponding asymptotical values obtained from a single fin as $S \to \infty$. The distributions of the fin temperature depart from the ideal isothermal situation and the fin temperature decreases more rapidly away from the circular center with increasing the fin spacing and air speed.

1. Introduction

The fins in heat exchangers are always applied to increase the heat flow per unit of basic surface. The analysis of a continuous plate fin pierced by a regularly spaced array of circular tubes in staggered and in-line arrays has many engineering applications. In order to simplify the problem considered, the calculation of the standard fin efficiency usually assumes that the heat transfer coefficient is constant over the plate fin. However, it is well known that there exists a very complex flow pattern within a plate finned-tube heat exchanger due to its three-dimensional natural and flow separations. The flow accelerates around a heated horizontal tube and forms a low-velocity wake region behind the tube. Thus the heat transfer coefficient is highest on the upstream fin region and is lowest on the wake fin region. This implies that the heat transfer coefficient on the fin is very non-uniform. On the other hand, the actual steady-state heat transfer coefficient on the fin inside a plate finned-tube heat exchanger should be the function of position. As shown in Ref. [1], the measurement of the local heat transfer coefficient on a plain fin under steady-state heat transfer conditions was very difficult to be performed, since the local fin temperature and heat flux were required. Thus the estimation of a more accurate heat transfer coefficient on the fin is an important task for the device of the high-performance heat exchangers.

Heat transfer coefficients encountered in forced convection are typically much higher than those encountered in natural convection because of the higher fluid velocities associated with forced convection. As a result, most of researchers tend to ignore natural convection in heat transfer analyses that involve forced convection, although it is known that natural convection always accompanies forced convection. However, this error may be considerable at low velocities associated with forced convection [2].

* Corresponding author. Fax: +886 6 235 2973.
E-mail address: htchen@mail.ncku.edu.tw (H.-T. Chen).

0017-9310/$ - see front matter © 2006 Elsevier Ltd. All rights reserved.
doi:10.1016/j.ijheatmasstransfer.2006.06.038

Nomenclature

A_f	area of the whole plate fin, m^2
A_j	area of the jth sub-fin region, m^2
$[A]$	global conduction matrix
d_o	outer diameter of a circular tube, m
$[F]$	force matrix
g	acceleration of gravity, m/s^2
Gr_d	Grashof number, $\frac{g\beta(T_o-T_\infty)d_o^3}{v^2}$
h	local heat transfer coefficient, W/m^2 K
$\bar{h}$	unknown average heat transfer coefficient on the whole plate fin, W/m^2 K
$\bar{h}_j$	unknown average heat transfer coefficient on the jth sub-fin region, W/m^2 K
k	thermal conductivity of the fin, W/m^2 K
k_{air}	thermal conductivity of the air, W/m K
L	side length of a square fin, m
ℓ	distance between two neighboring nodes in the x- and y-directions, m
m	dimensionless parameter defined in Eq. (5)
$\bar{m}_k$	unknown dimensionless parameter on the kth sub-fin region defined in Eq. (10)
N	number of sub-fin regions
Nu_d	Nusselt number defined in Eq. (36), $\frac{\bar{h}d_o}{k_{air}}$
N_x	number of nodes in the x-direction
N_y	number of nodes in the y-direction
Q	total heat rate dissipated from the whole plate fin, W
q_j	heat rate dissipated from the jth sub-fin region, W
Re_d	Reynolds number, $\frac{V_{air}d_o}{v}$
r_o	outer radius of a circular tube, m
S	fin spacing, m
S_1	outer boundary surface of the circular tube
T	fin temperature, K
T_j	temperature of the jth sub-fin region, K
T_o	outer surface temperature of the circular tube, K
T_∞	ambient temperature, K
V_{air}	frontal air speed, m/s
X, Y	spatial coordinates, m
x, y	dimensionless spatial coordinates

Greek symbols

β	volumetric thermal expansion coefficient, 1/K
δ	fin thickness, m
η_f	fin efficiency
v	kinematic viscosity of the air, m^2/s
θ	temperature difference shown in Eq. (6), K
$[\theta]$	global temperature matrix

Superscripts

cal	calculated value
mea	measured data

Quantitative studies of the heat transfer processes occurring in the industrial applications require accurate knowledge of the surface conditions and thermal physical quantities of the test material. It is known that these physical quantities and surface conditions can be predicted using the measured temperatures inside this test material. Such problems are called the inverse heat conduction problems. These inverse problems have become an interesting subject recently. To date, various inverse methods in conjunction with the measured temperatures inside the test material have been developed for the analysis of the inverse heat conduction problems [3,4]. However, to the authors' knowledge, a few researchers performed the prediction of the local heat transfer coefficients on a plate fin inside the plate finned-tube heat exchangers with regard for the effect of the fin spacing [5–12].

Jones and Russell [5] applied the transient technique to determine the local heat transfer coefficient on the rectangular fin pierced by an elliptical steel tube and then the finite element method was used to calculate its fin efficiency. Saboya and Sparrow [6] and Rosman et al. [7] cast solid naphthalene plates in the form of a plate-fin-and-tube flow passage and used mass transfer technique to infer the local heat transfer coefficient from the heat-mass transfer analogy. The local mass transfer coefficient was defined by measuring the thickness of naphthalene lost by sublimation during a timed test run. Recently, Ay et al. [8] performed an experimental study with the infrared thermovision to monitor the temperature distribution on a plate-fin surface inside the plate finned-tube heat exchangers and then the local heat transfer coefficient on the test fin can be determined using the obtained experimental temperature measurements. Huang et al. [9] applied the steepest descent method and a general purpose commercial code CFX4.4 to estimate the local heat transfer coefficients for the plate finned-tube heat exchangers based on the simulated measured temperature distribution on the fin surface by infrared thermography. However, the difference of the local heat transfer coefficients on the downstream and upstream fin regions and fin efficiency were not shown in the works of Ay et al. [8] and Huang et al. [9]. Sometimes, it is maybe difficult to measure the temperature distributions on the fin of plate finned-tube heat exchangers using the infrared thermography and thermocouples for some practical heat transfer problems. Due to this reason, Chen et al. [10] applied the inverse scheme of the finite difference method in conjunction with the least-squares scheme and experimental temperature data to predict the fin efficiency and average heat transfer coefficient on the fin inside one-tube plate finned-tube heat exchangers for a single fin and various air speeds. The experiment of this study [10] was made in an induced open wind tunnel. The setup of

this experiment was based on ASHRAE 41.2 standard. The tube temperature was assumed to be the average of the inlet and outlet water temperatures. The ambient temperatures at the inlet and exit zones across the test section were controlled by an air-ventilator and were measured by two psychometric boxes. The ambient temperature was the average of these two temperatures. Six K-type thermocouples welded at the suitable positions of the sub-fin regions were applied to measure the fin temperatures. The ambient airflow was driven by a 3.73 kW centrifugal fan with an inverter to provide various inlet velocities. The airflow measuring station was an outlet chamber setup with multiple nozzles based on ASHARE 41.1 standard. However, it seems to be difficult to measure the tube temperature, ambient temperature and air speed in the neighbor of the test specimen using this experimental apparatus. In order to evidence the accuracy of the predicted results, Chen and Chou [11] applied the same scheme to predict the natural-convection heat transfer coefficient and fin efficiency on the fin of one-tube finned-tube heat exchangers in a small open box for various fin spacings. It can be found that the predicted results of the average heat transfer coefficient given in Ref. [11] agreed with those obtained from the correlation recommended by current textbooks under the assumption of the ideal isothermal fin. Thus the present study applied the same inverse scheme [11] to predict the average heat transfer coefficient and fin efficiency on the fin of one-tube finned-tube heat exchangers in a small wind tunnel for various air speeds and fin spacings. Due to the difference of the measurement manner, comparison between the present estimates and those given in Ref. [10] can be difficult to be performed. Mon and Gross [12] applied the three-dimensional numerical study to investigate the effect of the fin spacing on four-row annular-finned tube bundles in staggered and in-line arrangements.

The inverse analysis of the present study is that the whole fin area is divided into several analysis sub-fin regions and then the fin temperatures at these selected measurement locations are measured using T-type thermocouples. Later, the finite difference method in conjunction with the temperature measurements and least-squares method is applied to predict the average heat transfer coefficients on these sub-fin regions. Furthermore, the average heat transfer coefficient on the whole plate fin $\bar{h}$ and fin efficiency can be obtained for various air speeds and fin spacings under the given conditions of the ambient and tube temperatures.

The advantage of the present study is that the governing differential equations for the airflow do not need to be solved. In this study, the effect of the air speed and fin spacing on the estimation of the $\bar{h}$ value is investigated. The computational procedures for the estimates of the heat transfer coefficients on each sub-fin region are performed repeatedly until the sum of the squares of the deviations between the calculated and measured temperatures becomes minimum.

2. Mathematical formulation

The experimental apparatus configuration of the small wind tunnel used in the present study is shown in Fig. 1. Fig. 2 shows the experimental configuration of the test square fin vertically mounted on a circular tube. The schematic diagram of one-tube plate finned-tube heat exchanger is shown in Fig. 3. Fig. 4 shows the physical model of the two-dimensional thin plate fin inside one-tube plate fin heat exchanger, where r_o, L and δ denote the outer radius of the circular tube, side length of the square plate fin and fin thickness, respectively. The center of the circular tube is located at $(L/2, L/2)$. T_o and T_∞ respectively denote the outer surface temperature of the circular tube and the ambient temperature. Due to the thin fin behavior, the temperature gradient in the z-direction (the fin thickness) is small and the fin temperature varies only in the X- and Y-directions. The "insulated tip" assumption can be an adequate approximation provided that the actual

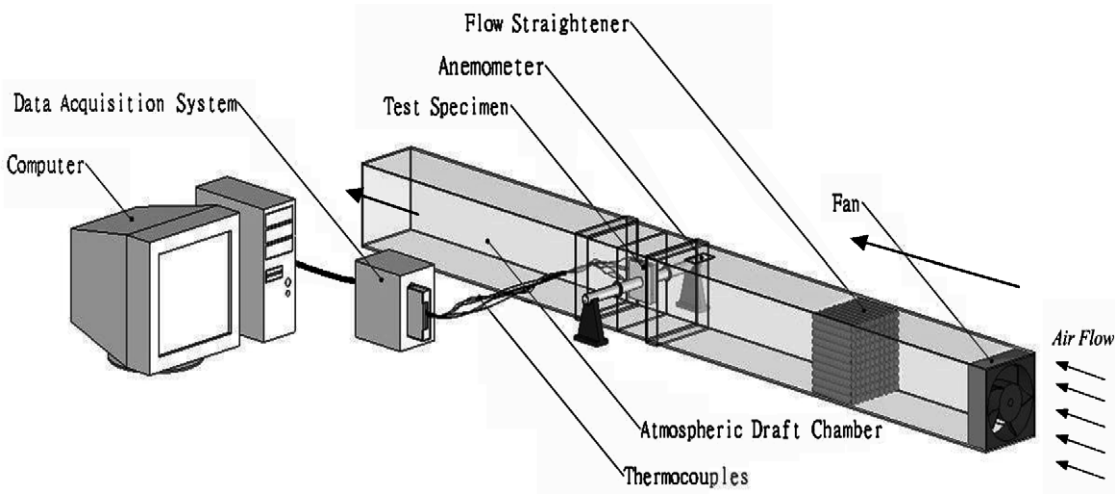

Fig. 1. Experimental apparatus configuration of the small wind tunnel used in the present study.

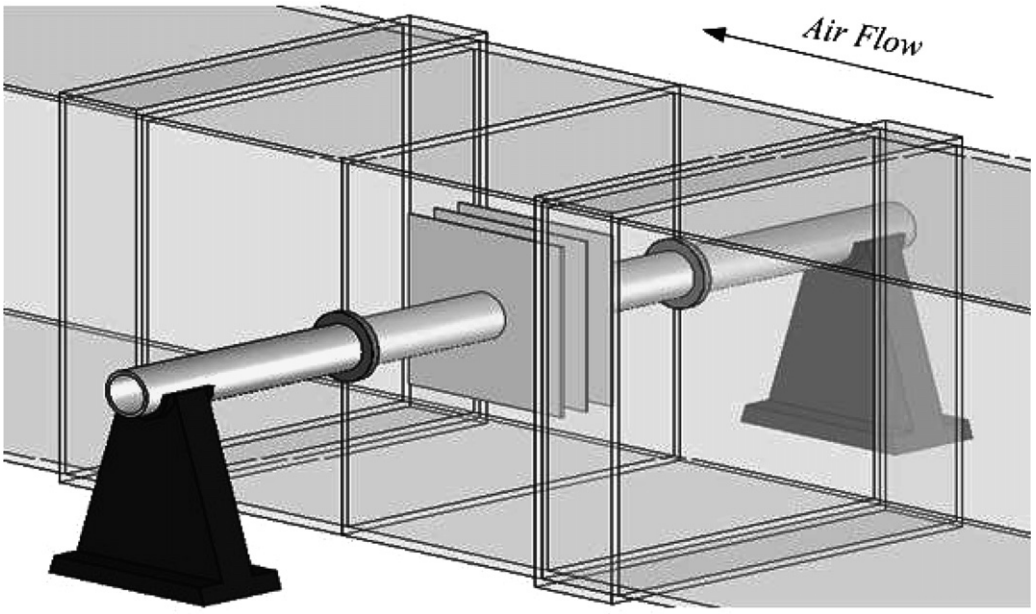

Fig. 2. Experimental configuration of the test square fin vertically mounted on a circular tube.

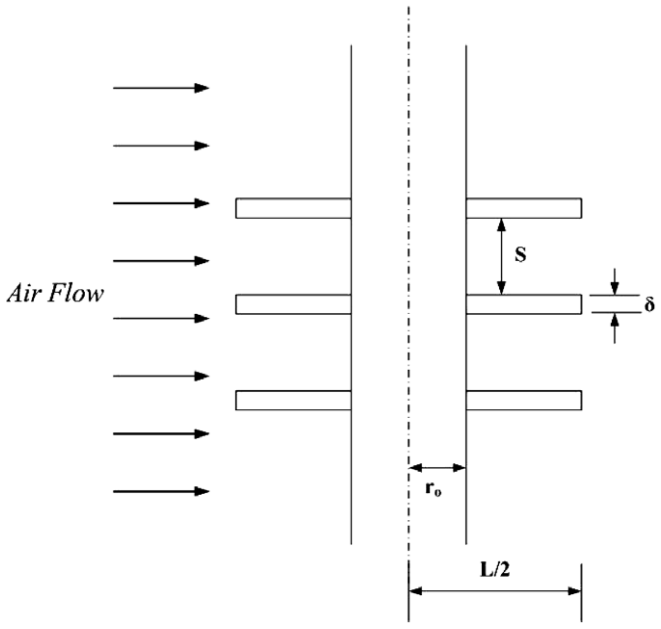

Fig. 3. Schematic diagram of one-tube plate fin heat exchangers with the fin spacing.

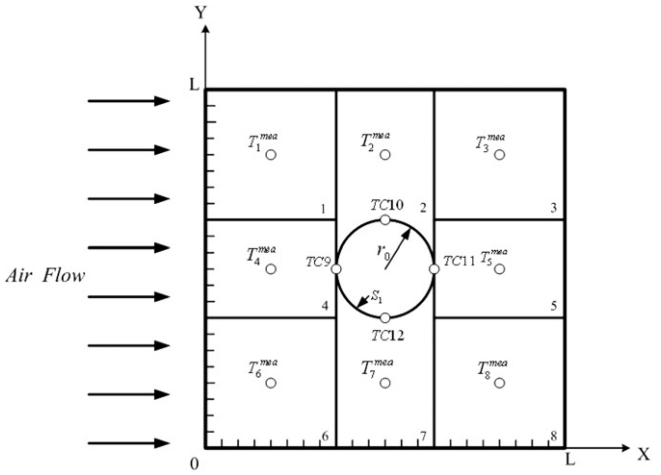

Fig. 4. Physical geometry of a two-dimensional plate fin with measurement locations and sub-fin regions.

heat rate dissipated through the tip is much smaller than the total heat rate drawn from the base wall [13]. It can be found from the works of Jones and Russell [5], Saboya and Sparrow [6], Rosman et al. [7] and Ay et al. [8] that the heat transfer coefficient on the fin of plate finned-tube heat exchangers in forced convection is very non-uniform. Thus the heat transfer coefficient $h(X, Y)$ in the present study is also assumed to be non-uniform. The heat transfer coefficient on the fin of plate finned-tube heat exchangers can be estimated provided that the fin temperatures at various measurement locations can be measured. Under the assumptions of the steady state and constant thermal properties, the two-dimensional heat conduction equation for the continuous thin fin of one-tube finned-tube heat exchangers can be expressed as

$$\frac{\partial^2 T}{\partial X^2}+\frac{\partial^2 T}{\partial Y^2}=\frac{2h(X,Y)}{k\delta}(T-T_\infty) \tag{1}$$

Its corresponding boundary conditions are

$$\frac{\partial T}{\partial X}=0 \quad \text{at } X=0 \text{ and } X=L \tag{2}$$

$$\frac{\partial T}{\partial Y}=0 \quad \text{at } Y=0 \text{ and } Y=L \tag{3}$$

$$T=T_{\mathrm{o}}\,(X,Y) \quad \text{on } S_1 \tag{4}$$

where T is the fin temperature. X and Y are Cartesian coordinates. S_1 denotes the boundary of the circular tube with radius r_o. k is the thermal conductivity of the fin.

For convenience of the inverse analysis, the following dimensionless parameters are introduced as:

$$x = X/L, \quad y = Y/L \quad \text{and} \quad m(x,y) = \frac{2L^2 h(X,Y)}{k\delta} \tag{5}$$

Substitution of Eq. (5) into Eqs. (1)–(4) gives the following equations:

$$\frac{\partial^2\theta}{\partial x^2} + \frac{\partial^2\theta}{\partial Y^2} = m(X,Y)\theta \tag{6}$$

$$\frac{\partial\theta}{\partial x} = 0 \quad \text{at } x = 0 \text{ and } x = 1 \tag{7}$$

$$\frac{\partial\theta}{\partial y} = 0 \quad \text{at } y = 0 \text{ and } y = 1 \tag{8}$$

and

$$\theta = \theta_0 \quad (X,Y) \quad \text{on } S_1 \tag{9}$$

where $\theta = T - T_\infty$.

3. Numerical analysis

In the present study, the whole plate fin is divided into N sub-fin regions. The heat transfer coefficient on each sub-fin region is assumed to be constant. Thus the application of the finite difference method to Eq. (6) can produce the following difference equation on the kth sub-fin region as

$$\frac{\theta_{i+1,j} - 2\theta_{i,j} + \theta_{i-1,j}}{\ell^2} + \frac{\theta_{i,j+1} - 2\theta_{i,j} + \theta_{i,j-1}}{\ell^2} = \bar{m}_k\theta_{i,j} \quad \text{for } k = 1,2,\ldots,N \tag{10}$$

where ℓ is the distance between two neighboring nodes in the x- and y-directions and is defined as $\ell = 1/(N_x - 1) = 1/(N_y - 1)$, where N_x and N_y are the nodal numbers in x- and y-directions, respectively. $\bar{m}_k$ denotes the unknown dimensionless parameter on the kth sub-fin region and is defined as $\bar{m}_k = 2L^2\bar{h}_k/(k\delta)$, where $\bar{h}_k$ denotes the average heat transfer coefficient on the kth sub-fin region.

The application of the central difference approximation to the boundary conditions (7) and (8) can yield their approximate forms as

$$\theta_{2,j} = \theta_{0,j} \quad \text{and} \quad \theta_{N_x-1,j} = \theta_{N_x+1,j} \quad \text{for } j = 1,2,\ldots,N_y \tag{11}$$

$$\theta_{i,2} = \theta_{i,0} \quad \text{and} \quad \theta_{i,N_y-1} = \theta_{i,N_y+1} \quad \text{for } i = 1,2,\ldots,N_x \tag{12}$$

Substitution of Eqs. (11) and (12) into their corresponding difference equations can obtain the difference equations at the boundary surfaces as

$$\frac{2\theta_{2,j} - 2\theta_{1,j}}{\ell^2} + \frac{\theta_{1,j+1} - 2\theta_{1,j} + \theta_{1,j-1}}{\ell^2} = \bar{m}_k\theta_{1,j} \quad \text{for } k = 1,4,6 \tag{13}$$

$$\frac{-2\theta_{N_x,j} + 2\theta_{N_x-1,j}}{\ell^2} + \frac{\theta_{N_x,j+1} - 2\theta_{N_x,j} + \theta_{N_x,j-1}}{\ell^2} = \bar{m}_k\theta_{N_x,j} \quad \text{for } k = 3,5,8 \tag{14}$$

$$\frac{\theta_{i+1,1} - 2\theta_{i,1} + \theta_{i-1,1}}{\ell^2} + \frac{2\theta_{i,2} - 2\theta_{i,1}}{\ell^2} = \bar{m}_k\theta_{i,1} \quad \text{for } k = 6,7,8 \tag{15}$$

and

$$\frac{\theta_{i+1,N_y} - 2\theta_{i,N_y} + \theta_{i-1,N_y}}{\ell^2} + \frac{-2\theta_{i,N_y} + 2\theta_{i,N_y-1}}{\ell^2} = \bar{m}_k\theta_{i,N_y} \quad \text{for } k = 1,2,3 \tag{16}$$

It can be found from Refs. [14,15] that the boundary of the circular tube may be approximated using an octagon in terms of a Cartesian coordinate system. Thus a more accurate modified difference equation based on this technique can be constructed in the present study.

The difference equations for the nodes at the interface of two neighboring sub-fin regions, as shown in Fig. 5, can be expressed as

$$\frac{\theta_{i+1,j} - 2\theta_{i,j} + \theta_{i-1,j}}{\ell^2} + \frac{\theta_{i,j+1} - 2\theta_{i,j} + \theta_{i,j-1}}{\ell^2} = \frac{\bar{m}_k + \bar{m}_{k^*}}{2}\theta_{i,j} \tag{17}$$

where $\bar{m}_{k^*}$ denotes the unknown dimensionless parameter on the k^*th sub-fin region and is defined as $\bar{m}_{k^*} = 2L^2\bar{h}_{k^*}/(k\delta)$, where $\bar{h}_{k^*}$ denotes the average heat transfer coefficient on the k^*th sub-fin region.

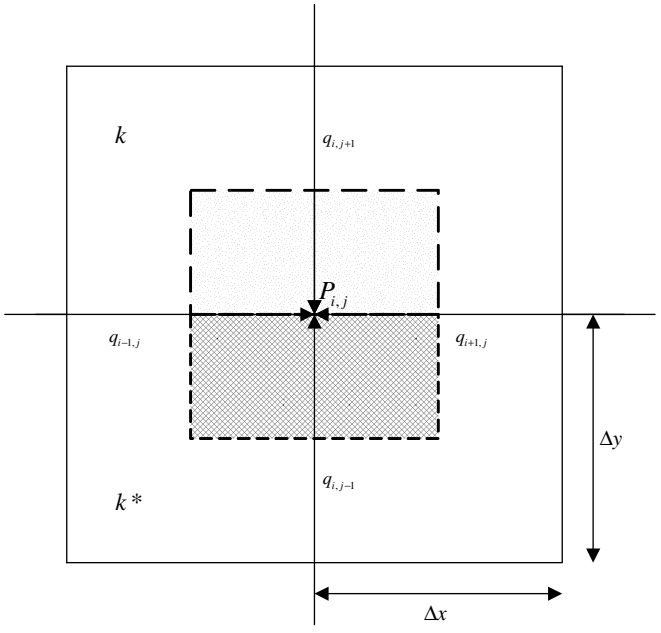

Fig. 5. Nodes for the interface of two-neighboring sub-fin areas.

Rearrangement of Eq. (10) and Eqs. (13)–(17) in conjunction with the difference equations in the neighboring of the circular tube can yield the following matrix equation:

$$[A][\theta] = [F] \tag{18}$$

where $[A]$ is a global conduction matrix. $[\theta]$ is a matrix representing the nodal temperatures. $[F]$ is a force matrix. The nodal temperatures can be obtained from Eq. (18) using the Gauss elimination method.

However, it is maybe difficult to measure the temperature distributions on the whole square plate fin using the infrared thermography and thermocouples for some practical heat transfer problems. Relatively, the unknown heat transfer coefficient on the fin $h(x,y)$ is not easy to be obtained. Under this circumstance, the whole square plate fin considered can be divided into several sub-fin regions in the present inverse scheme and then the unknown heat transfer coefficient on each sub-fin region can be approximated by a constant value. Under this assumption, the heat rate dissipated from this sub-fin region q_j is

$$q_j = 2\bar{h}_j \int_{A_j} (T - T_\infty)\,\mathrm{d}A \quad \text{for } j = 1,2,\ldots,N \tag{19}$$

The average heat transfer coefficient on the whole plate fin $\bar{h}$ can be expressed as

$$\bar{h} = \sum_{j=1}^{N} \bar{h}_j A_j / A_f \tag{20}$$

where N is the number of the sub-fin regions. A_f is the area of the whole square plate fin.

The efficiency of the square plate fin η_f is defined as the ratio of the actual heat transfer from the square plate fin to the dissipated heat from the fin maintained at the tube temperature T_o. Thus the fin efficiency η_f can be expressed as

$$\eta_f = \frac{\sum_{j=1}^{N} q_j}{2A_f(T_o - T_\infty)\bar{h}} \tag{21}$$

The total heat rate dissipated from the whole square plate fin to the ambient Q can be written as

$$Q = \sum_{j=1}^{N} q_j \tag{22}$$

In order to estimate the unknown heat transfer coefficient on the jth sub-fin region $\bar{h}_j$, the additional information of the steady-state measured temperatures is required at N interior measurement locations. The more a number of the sub-fin regions are, the more accurate the estimation of the unknown average heat transfer coefficient on the whole square plate fin is. Relatively, a more computational time can be required. In the present study, T-type thermocouples are used to record the temperature information at selected measurement locations. The measured temperature taken from the jth thermocouple is denoted by T_j^{mea}, $j = 1,\ldots,N$, as shown in Tables 1 and 2.

The least-squares minimization technique is applied to minimize the sum of the squares of the deviations between the calculated and measured temperatures at selected measurement locations. The error in the estimates $E(\bar{m}_1, \bar{m}_2, \ldots, \bar{m}_N)$ is minimized and is defined as

$$E(\bar{m}_1, \bar{m}_2, \ldots, \bar{m}_N) = \sum_{j=1}^{N} \left[\theta_j^{\mathrm{cal}} - \theta_j^{\mathrm{mea}}\right]^2 \tag{23}$$

where the unknown average heat transfer coefficients on each sub-fin region $\bar{h}_i$, $i = 1,2,\ldots,N$, can be obtained from the definition of $\bar{m}_i$. The calculated temperature taken from the jth thermocouple location, θ_j^{cal}, is taken from Eq. (18). The temperature θ_j^{mea} is defined as $\theta_j^{\mathrm{mea}} = T_j^{\mathrm{mea}} - T_\infty$.

The estimated values of $\bar{m}_i, i = 1,2,\ldots,N$, are determined until the value of $E(\bar{m}_1, \bar{m}_2, \ldots, \bar{m}_N)$ is minimum. The computational procedures for estimating the $\bar{m}_i$ value, $i = 1,2,\ldots,N$, are described as follows.

First, the initial guesses of $\bar{m}_i, i = 1,2,\ldots,N$, are arbitrarily chosen. Later, the calculated temperature θ_j^{cal}, can be determined. Deviation of θ_j^{mea} and θ_j^{cal}, e_j, is expressed as

$$e_j = \theta_j^{\mathrm{cal}} - \theta_j^{\mathrm{mea}} \quad \text{for } j = 1,2,\ldots,N \tag{24}$$

The new calculated temperature $\theta_j^{\mathrm{cal},n}$ can be expanded in a first-order Taylor series as

$$\theta_j^{\mathrm{cal},n} = \theta_j^{\mathrm{cal}} + \sum_{i=1}^{N} \frac{\partial \theta_j^{\mathrm{cal}}}{\partial \bar{m}_i}\,\mathrm{d}\bar{m}_i \quad \text{for } j = 1,2,\ldots,N \tag{25}$$

In order to obtain the $\frac{\partial \theta_j^{\mathrm{cal}}}{\partial \bar{m}_i}$ value, the new estimated value $\bar{m}_i^*$ is introduced and is expressed as

$$\bar{m}_i^* = \bar{m}_i + d_i\delta_{ik} \quad \text{for } i,k = 1,2,\ldots,N \tag{26}$$

where $d_i = \bar{m}_i^* - \bar{m}_i$ denotes the correction. The symbol δ_{jk} is Kronecker delta.

Accordingly, the new calculated temperature $\theta_j^{\mathrm{cal},n}$ with respect to $\bar{m}_i^*$ can be determined from Eq. (18). Deviation of $\theta_j^{\mathrm{cal},n}$ and θ_j^{mea}, e_j^n, can be defined as

$$e_j^n = \theta_j^{\mathrm{cal},n} - \theta_j^{\mathrm{mea}} \quad \text{for } j = 1,2,\ldots,N \tag{27}$$

The finite difference representation of the derivative $\frac{\partial \theta_j^{\mathrm{cal}}}{\partial \bar{m}_i}$ can be expressed as

$$\omega_j^i = \frac{\partial \theta_j^{\mathrm{cal}}}{\partial \bar{m}_i} = \frac{\theta_j^{\mathrm{cal},n} - \theta_j^{\mathrm{cal}}}{\bar{m}_i^* - \bar{m}_i} \quad \text{for } j = 1,2,\ldots,N \tag{28}$$

Substitution of Eqs. (24), (26) and (27) into Eq. (28) can yield

$$\omega_j^i = \frac{e_j^n - e_j}{d_i} \quad \text{for } j = 1,2,\ldots,N \tag{29}$$

Substitution of Eq. (28) into Eq. (25) can obtain the new expression of $\theta_j^{\mathrm{cal},n}$ as

Table 1
Temperature measurements and the present estimates for $V_{air} = 1$ m/s and various T_o, T_∞ and S values

	$S = 0.005$ m	$S = 0.01$ m	$S = 0.015$ m	$S \to \infty$
	$T_o = 338.6$ K $T_\infty = 298.2$ K	$T_o = 340.1$ K $T_\infty = 298.3$ K	$T_o = 340.1$ K $T_\infty = 297.5$ K	$T_o = 338.2$ K $T_\infty = 298.7$ K
T_j^{mea} (K)	$T_1^{mea} = 301.2$ $T_2^{mea} = 307.5$ $T_3^{mea} = 307.9$ $T_4^{mea} = 301.1$ $T_5^{mea} = 313.2$ $T_6^{mea} = 298.4$ $T_7^{mea} = 302.5$ $T_8^{mea} = 306.5$	$T_1^{mea} = 302.4$ $T_2^{mea} = 307.9$ $T_3^{mea} = 308.2$ $T_4^{mea} = 301.3$ $T_5^{mea} = 311.8$ $T_6^{mea} = 299.3$ $T_7^{mea} = 304.3$ $T_8^{mea} = 305.6$	$T_1^{mea} = 299.9$ $T_2^{mea} = 305.7$ $T_3^{mea} = 305.3$ $T_4^{mea} = 299.6$ $T_5^{mea} = 310.1$ $T_6^{mea} = 299.1$ $T_7^{mea} = 303.1$ $T_8^{mea} = 303.7$	$T_1^{mea} = 300.6$ $T_2^{mea} = 306.9$ $T_3^{mea} = 307.7$ $T_4^{mea} = 300.5$ $T_5^{mea} = 314.6$ $T_6^{mea} = 299.9$ $T_7^{mea} = 304.7$ $T_8^{mea} = 304.8$
$\bar{h}_j$ (W/m^2 K)	$\bar{h}_1 = 24.884$ $\bar{h}_2 = 40.37$ $\bar{h}_3 = 7.138$ $\bar{h}_4 = 145.41$ $\bar{h}_5 = 15.28$ $\bar{h}_6 = 68.42$ $\bar{h}_7 = 54.13$ $\bar{h}_8 = 8.86$	$\bar{h}_1 = 14.025$ $\bar{h}_2 = 42.56$ $\bar{h}_3 = 5.25$ $\bar{h}_4 = 147.38$ $\bar{h}_5 = 22.51$ $\bar{h}_6 = 75.21$ $\bar{h}_7 = 72.28$ $\bar{h}_8 = 8.64$	$\bar{h}_1 = 29.912$ $\bar{h}_2 = 49.62$ $\bar{h}_3 = 9.48$ $\bar{h}_4 = 187.13$ $\bar{h}_5 = 23.79$ $\bar{h}_6 = 37.13$ $\bar{h}_7 = 80.12$ $\bar{h}_8 = 11.97$	$\bar{h}_1 = 39.935$ $\bar{h}_2 = 45.67$ $\bar{h}_3 = 9.09$ $\bar{h}_4 = 216.84$ $\bar{h}_5 = 8.00$ $\bar{h}_6 = 58.22$ $\bar{h}_7 = 66.87$ $\bar{h}_8 = 18.01$
q_j (W)	$q_1 = 0.25$ $q_2 = 0.97$ $q_3 = 0.19$ $q_4 = 2.15$ $q_5 = 0.52$ $q_6 = 0.41$ $q_7 = 1.09$ $q_8 = 0.21$	$q_1 = 0.18$ $q_2 = 1.07$ $q_3 = 0.15$ $q_4 = 2.56$ $q_5 = 0.72$ $q_6 = 0.40$ $q_7 = 1.32$ $q_8 = 0.18$	$q_1 = 0.26$ $q_2 = 1.12$ $q_3 = 0.22$ $q_4 = 2.66$ $q_5 = 0.72$ $q_6 = 0.25$ $q_7 = 1.43$ $q_8 = 0.22$	$q_1 = 0.28$ $q_2 = 0.99$ $q_3 = 0.23$ $q_4 = 2.74$ $q_5 = 0.27$ $q_6 = 1.05$ $q_7 = 0.92$ $q_8 = 0.35$
$\bar{h}$ (W/m^2 K)	43.02	45.44	49.40	54.08
Q (W)	5.80	6.27	6.87	6.84
η_f	0.18	0.18	0.18	0.17

$$\theta_j^{cal,n} = \theta_j^{cal} + \sum_{i=1}^{N} \omega_j^i d_i^* \quad \text{for } j = 1, 2, \ldots, N \tag{30}$$

where $d_i^* = d\bar{m}_i$ denotes the new correction of the $\bar{m}_i$ value.

Substituting Eqs. (24) and (27) into Eq. (30) gives

$$e_j^n = e_j + \sum_{i=1}^{N} \omega_j^i d_i^* \quad \text{for } j = 1, 2, \ldots, N \tag{31}$$

As shown in Eq. (23), the error in the estimates $E(\bar{m}_1+\Delta\bar{m}_1, \bar{m}_2+\Delta\bar{m}_2, \ldots, \bar{m}_N + \Delta\bar{m}_N)$ can be expressed as

$$\mathbf{E} = \sum_{j=1}^{N} (e_j^n)^2 \tag{32}$$

In order to yield the minimum value of **E** with respect to the $\bar{m}_i$ values,, $i = 1, 2, \ldots, N$, differentiating **E** with respect to the new correction d_i^* will be performed. Thus the correction equations for the $\bar{m}_i$ values can be expressed as

$$\sum_{j=1}^{N} \sum_{k=1}^{N} \omega_k^i \omega_k^j d_j^* = -\sum_{j=1}^{N} \omega_j^i e_j, \quad i = 1, 2, \ldots, N \tag{33}$$

Eq. (33) is a set of N algebraic equations for the new corrections d_i^*. The new correction d_i^* can be obtained by solving Eq. (33). Furthermore, the new estimated heat transfer coefficients can also be determined. The above procedures are repeated until the values of $|\frac{\theta_j^{mea} - \theta_j^{cal}}{\theta_j^{mea}}|$, $j = 1, 2, \ldots, N$, are all less than 10^{-4}.

4. Experimental apparatus

The schematic diagram of the experimental apparatus used in the present study for the estimation of the forced-convection heat transfer coefficient on a square plate fin of one-tube plate finned-tube heat exchangers is shown in Fig. 1. This experiment is conducted in a small wind tunnel, as shown in Fig. 1. This wind tunnel with 226 cm in length, 22 cm in width and 22 cm in height is made of acrylic-plastic sheets. The ambient airflow was driven by a 115V-AC rotary fan with a 200 W dimmer switch to provide various inlet air speeds. During an experiment, the airflow is straightened by the flow straightener installed in the air inlet of the small wind tunnel. This flow straightener is constructed by many pipettes with 6 mm in diameter and 220 mm in length. An anemometer installed at 300 mm in front of the airflow entering the test specimen is used to measure the frontal air velocity. The horizontal circular tube with an outer diameter of 27.3 mm and 2 mm in thickness and the test square fin with 100 mm in length, 100 mm in width and 1 mm in thickness are made of AISI 304 stainless material. It can be found from Ref. [15] that

Table 2
Temperature measurements and the present estimates for $V_{air} = 3$ m/s and various T_o, T_∞ and S values

	$S = 0.005$ m	$S = 0.01$ m	$S = 0.015$ m	$S \to \infty$
	$T_o = 337.0$ K $T_\infty = 298.0$ K	$T_o = 335.0$ K $T_\infty = 297.7$ K	$T_o = 335.3$ K $T_\infty = 297.4$ K	$T_o = 336.5$ K $T_\infty = 297.7$ K
T_j^{mea} (K)	$T_1^{mea} = 299.9$ $T_2^{mea} = 303.4$ $T_3^{mea} = 303.2$ $T_4^{mea} = 299.5$ $T_5^{mea} = 307.7$ $T_6^{mea} = 298.6$ $T_7^{mea} = 300.8$ $T_8^{mea} = 302.9$	$T_1^{mea} = 299.4$ $T_2^{mea} = 303.5$ $T_3^{mea} = 302.8$ $T_4^{mea} = 298.7$ $T_5^{mea} = 306.6$ $T_6^{mea} = 298.4$ $T_7^{mea} = 301.5$ $T_8^{mea} = 302.3$	$T_1^{mea} = 299.2$ $T_2^{mea} = 304.3$ $T_3^{mea} = 303.2$ $T_4^{mea} = 298.8$ $T_5^{mea} = 307.4$ $T_6^{mea} = 297.6$ $T_7^{mea} = 301.1$ $T_8^{mea} = 301.9$	$T_1^{mea} = 299.1$ $T_2^{mea} = 303.0$ $T_3^{mea} = 304.0$ $T_4^{mea} = 298.6$ $T_5^{mea} = 311.1$ $T_6^{mea} = 298.5$ $T_7^{mea} = 301.4$ $T_8^{mea} = 301.1$
$\bar{h}_j$ (W/m^2 K)	$\bar{h}_1 = 25.542$ $\bar{h}_2 = 75.97$ $\bar{h}_3 = 12.63$ $\bar{h}_4 = 231.07$ $\bar{h}_5 = 31.83$ $\bar{h}_6 = 63.45$ $\bar{h}_7 = 145.07$ $\bar{h}_8 = 8.58$	$\bar{h}_1 = 27.955$ $\bar{h}_2 = 65.10$ $\bar{h}_3 = 12.67$ $\bar{h}_4 = 303.43$ $\bar{h}_5 = 35.51$ $\bar{h}_6 = 74.09$ $\bar{h}_7 = 103.11$ $\bar{h}_8 = 11.56$	$\bar{h}_1 = 44.563$ $\bar{h}_2 = 55.20$ $\bar{h}_3 = 13.78$ $\bar{h}_4 = 323.04$ $\bar{h}_5 = 30.11$ $\bar{h}_6 = 58.51$ $\bar{h}_7 = 122.79$ $\bar{h}_8 = 15.24$	$\bar{h}_1 = 33.849$ $\bar{h}_2 = 76.36$ $\bar{h}_3 = 13.06$ $\bar{h}_4 = 332.72$ $\bar{h}_5 = 9.03$ $\bar{h}_6 = 90.01$ $\bar{h}_7 = 105.92$ $\bar{h}_8 = 32.19$
q_j (W)	$q_1 = 0.17$ $q_2 = 1.26$ $q_3 = 0.20$ $q_4 = 2.69$ $q_5 = 0.78$ $q_6 = 0.23$ $q_7 = 1.72$ $q_8 = 0.12$	$q_1 = 0.14$ $q_2 = 1.08$ $q_3 = 0.19$ $q_4 = 3.09$ $q_5 = 0.82$ $q_6 = 0.25$ $q_7 = 1.36$ $q_8 = 0.16$	$q_1 = 0.23$ $q_2 = 0.97$ $q_3 = 0.22$ $q_4 = 3.21$ $q_5 = 0.72$ $q_6 = 0.20$ $q_7 = 1.49$ $q_8 = 0.19$	$q_1 = 0.18$ $q_2 = 1.25$ $q_3 = 0.24$ $q_4 = 3.34$ $q_5 = 0.26$ $q_6 = 0.28$ $q_7 = 1.37$ $q_8 = 0.39$
$\bar{h}$ (W/m^2 K)	68.32	72.57	76.00	80.49
Q (W)	7.16	7.07	7.22	7.30
η_f	0.15	0.14	0.14	0.13

the thermal conductivity of AISI 304 stainless material is 14.9 W/m K. The horizontal circular tube is placed on two wood supporters, which is 98 mm above an experimental table to prevent ground effects. The test fins are vertically mounted on this circular tube, as shown in Figs. 1 and 2. The ambient and test fin temperatures are measured using T-type thermocouples. A cylindrical rod with an outer diameter of 20 mm and 100 mm in length bound by a single thermofoil heater with an outer diameter of 1.5 mm is inserted in the circular tube and then the tube will be heated. Thus the radial gap between the surrounding circular tube and the whole electrical heating rod is small. On the other hand, the whole electrical heating rod is nearly fitted to the surrounding circular tube. Two hundred Watt power input was supplied the heater. The electrical heating rod was heated about 2 h. However, the steady-state condition has reached about 2000 s. The readings of all the thermocouples used to measure the ambient temperature, tube temperature and fin temperature are recorded from $t = 0$ until the steady-state condition has reached. All the data signals were collected and converted by a data acquisition system (National Instruments NI SCXI-1000, 1102 and 1300). The data acquisition system then transmitted the converted signals through a DAQ interface to a personal computer in conjunction with the Labview software for further operation. The limit of error of the thermocouple is ±0.4%. The histories of the measured temperatures for all the thermocouples are obtained using a curve-fitted scheme. The experiment will be repeatedly made provided that one of the temperature measurements for all the thermocouples is not very accurate. In order to check the accuracy of the measured temperatures, the experiments are at least repeated 2 times. In order to minimize the effect of the thermal contact resistance between the fin and circular tube on the estimates, the gap between the fin and the circular tube is filled with the cyanoacrylate adhesive (Satlon, D-3). In addition, four thermocouples placed in the interface between the fin and circular tube are fixed at four different positions of the fin base, TC9, TC10, TC11 and TC12 shown in Fig. 4, by using a cyanoacrylate adhesive (Satlon, D-3). The fin base temperature is measured from these four thermocouples. The average of these four temperature measurements is taken as the fin base temperature and is also assumed to be the outer surface temperature of the circular tube T_o in the present study. Three thermocouples penetrated the central line of the top surface and two lateral surfaces are positioned at 100 mm away from the test specimen in order to measure the ambient temperature T_∞. The average of these three temperature measurements is taken as the ambient temperature T_∞. For the present problem, the flow and thermal fields in the previous works were often

assumed to be symmetric. In order to investigate the reliability of the above assumption, the regular arrangements of the thermocouples welded on the square fin are chosen. Thus the whole square fin is divided into eight sub-fin regions, i.e., $N = 8$. Regions 1, 2 and 3 are the fin regions above the tube. Regions 6, 7 and 8 are the fin regions below the tube. In order to estimate the average heat transfer coefficient on each sub-fin region, eight T-type thermocouples are welded at the suitable positions of these sub-fin regions, as shown in Fig. 4. Eight T-type thermocouples for the measurements of the fin temperature are respectively welded at (2/11, 9/11), (1/2, 9/11), (9/11, 9/11), (2/11, 1/2), (9/11, 1/2), (2/11, 2/11), (1/2, 2/11) and (9/11, 2/11). The values of T_1^{mea} (2/11, 9/11), T_2^{mea} (1/2, 9/11), T_3^{mea} (9/11, 9/11), T_4^{mea} (2/11, 1/2), T_5^{mea} (9/11, 1/2), T_6^{mea} (2/11, 2/11), T_7^{mea} (1/2, 2/11) and T_8^{mea} (9/11, 2/11), respectively denote T_1^{mea}, T_2^{mea}, T_3^{mea}, T_4^{mea}, T_5^{mea}, T_6^{mea}, T_7^{mea} and T_8^{mea}. It can be observed that the first, second, third, sixth, seventh and eighth thermocouples are symmetric with respect to $y = 1/2$. The diameter of the spot sizes of eight thermocouples is about 0.13 mm.

5. Results and discussion

It can be observed from Ref. [13] that the "insulated tip" assumption is a good approximation when the actual heat rate passed through the tip is negligible relative to the total heat rate drawn from the base wall. For simplicity, the average heat transfer coefficient on the tip surface can be assumed to be the same as that on the lateral surfaces of the fin. On the other hand, the "insulated tip" assumption will be reasonable provided that the surface area of the fin tip is very smaller than the total fin surface area. Their ratio for the present study can be written as $\frac{2\delta L}{(L^2-\pi r_o^2)+2\delta L}$. Based on the experiment data given in the present study, the surface area of the fin tip is only 2.08% of the total fin surface area. This implies that the heat rate passed through the fin tip can be neglected in the present study. Thus Eqs. (2) and (3) in the present study should be the reasonable assumptions. In this study, the Reynolds number Re_d is defined as $Re_d = V_{\text{air}} d_o/\nu$, where V_{air}, d_o and ν denote the frontal air speed, outer diameter of the circular tube and kinematic viscosity of the air. It is well known that the parameter Gr_d/Re_d^2 represents the importance of natural convection and forced convection for a given fluid, where Gr_d denotes the Grashof number and is defined as $Gr_d = \frac{g\beta(T_o - T_\infty)d_0^3}{\nu^2}$. The property β in the Grashof number denotes the expansion coefficient of the air.

The temperature measurements T_1^{mea}, T_2^{mea}, T_3^{mea}, T_4^{mea}, T_5^{mea}, T_6^{mea}, T_7^{mea} and T_8^{mea} at $V_{\text{air}} = 1$ m/s and 3 m/s are respectively shown in Tables 1 and 2 for various T_o, T_∞ and S values. The nodal numbers N_x and N_y used in the computation are $N_x = N_y = 23$. Tables 1 and 2 also show the effect of the fin spacing S on the average heat transfer coefficient on the jth sub-fin region $\bar{h}_j$, heat rate on the jth sub-fin region q_j, total heat rate on the whole square fin Q, average heat transfer coefficient on the whole square fin $\bar{h}$ and fin efficiency η_f. An interesting finding that is $T_1^{\text{mea}} \neq T_6^{\text{mea}}$, $T_2^{\text{mea}} \neq T_7^{\text{mea}}$ and $T_3^{\text{mea}} \neq T_8^{\text{mea}}$ can be observed from Tables 1 and 2. This phenomenon can result from the following reasons that the flow pattern behind the tube may become turbulent and random in motion for the present problem and the test specimen can not be easy to be horizontally positioned. Thus the symmetric assumptions of the flow and thermal fields are not always very reasonable for the present real problem. Due to the heated air arising above the horizontal circular, it can be found from Tables 1 and 2 that the measured temperatures on the fin regions above the tube, T_1^{mea}, T_2^{mea} and T_3^{mea}, respectively are higher than those on the fin regions above the tube, T_6^{mea}, T_7^{mea} and T_8^{mea}.

Due to the blockade of the tube, the airflow coming into the region between two parallel fins accelerates around a hot horizontal tube and forms a low-velocity wake region behind the tube. Thus it can be found from Tables 1 and 2 that the fin temperatures on the downstream fin region are markedly higher than those on the upstream fin region for various T_o, T_∞ and S values. The same phenomenon can also be found from Ref. [10]. This result causes that the maximum heat transfer coefficient and heat flux occur on the front fin region. On the other hand, Region 4 makes a big contribution to the whole heat transfer coefficient. In general, the average heat transfer coefficients on the downstream sub-fin regions behind the tube are lower than those on the other sub-fin regions, as shown in Tables 1 and 2. On the other hand, these regions belong to the low-performance wake region. Moreover, the average heat transfer coefficients on Regions 2 and 7 are larger than those on the downstream sub-fin regions due to the formation of recirculating flow. Therefore, in order to enhance the overall heat transfer, it is worth to find a way to increase heat transfer in these regions. This may lead to design a heat exchanger with a high heat transfer performance. The ratio of the average heat transfer coefficient on the front fin region $\bar{h}_4$ to that on the wake fin region $\bar{h}_5$ for $S = 0.005$ m is up to 10 times at $V_{\text{air}} = 1$ m/s and is about 7 times at $V_{\text{air}} = 3$ m/s. It can be observed from Ref. [7] that the heat transfer coefficient is low on the back fin region of the tube and is much higher on the entrance fin region than on the wake fin region. It is obvious that the present results agree with those given by Rosman et al. [7]. The ratio of the heat flux on the front fin region q_4 to that on the wake fin region q_5 for $S = 0.005$ m is about 4 times at $V_{\text{air}} = 1$ m/s and is about 3.5 times at $V_{\text{air}} = 3$ m/s. The results in Tables 1 and 2 show that the wake fin region of a one-tube finned-tube heat exchanger in the range of $V_{\text{air}} = 1$–3 m/s is responsible for 10% of the total heat rate on the whole plate fin when $0.005\text{ m} \leqq S \leqq 0.015$ m. It is worth noting that the average heat transfer coefficient on the jth sub-fin region $\bar{h}_j, j = 1, 2, \ldots, 8$, are a little sensitive to the measured fin temperatures at various measurement locations. However, the average heat transfer coefficient $\bar{h}$ seems to be not very sensitive to the measured fin temperatures at various measurement locations.

It can be observed from Tables 1 and 2 that the average heat transfer coefficient $\bar{h}$ increases with increasing the fin spacing S and air speed V_{air}, and the fin efficiency η_f decreases with increasing the S and V_{air}. However, the effect of S on $\bar{h}$ and η_f were not discussed in the works of Rosman et al. [7] and Ay et al. [8]. The $\bar{h}$ value in the range of $V_{air} = 1$–3 m/s increases from 43.02 W/m^2 K to 68.32 W/m^2 K for $S = 0.005$ m and from 49.40 W/m^2 K to 76.00 W/m^2 K for $S = 0.015$ m. The η_f value decreases from 18% to 15% for $S = 0.005$ m and from 18% to 14% for $S = 0.015$ m. Figs. 6 and 7 respectively show the variations of the $\bar{h}$ and η_f values with the fin spacing for various V_{air} values. It can be found from Figs. 6 and 7 that the $\bar{h}$ and η_f values respectively approach their corresponding asymptotical values obtained from a single square fin as $S \to \infty$. The effect of the fin spacing S on the $\bar{h}$ and η_f values shown in Figs. 6 and 7 can be negligible when the S value exceeds about 0.03 m. The similar phenomenon can also be observed from Ref. [11]. This implies that the present estimated results are reasonable and are obtained over a reasonably wide range of fin spacings.

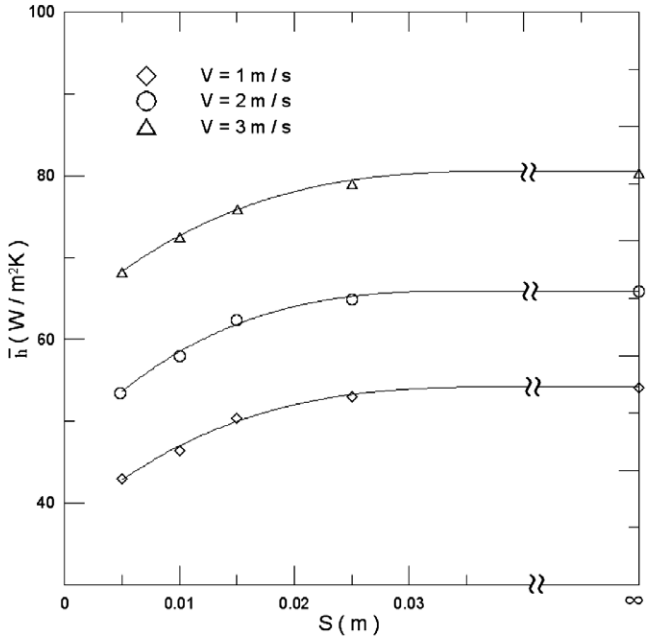

Fig. 6. Variation of $\bar{h}$ with S for various V_{air} values.

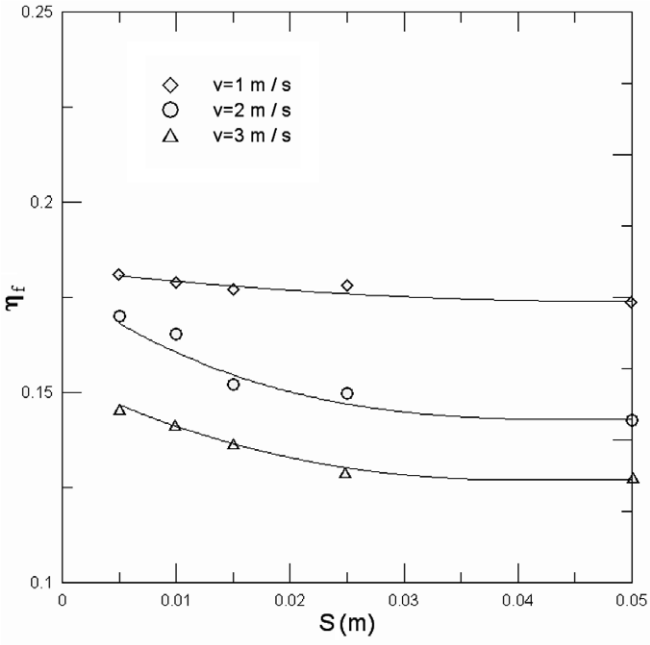

Fig. 7. Variation of η_f with S for various V_{air} values.

Once the average heat transfer coefficient on each sub-fin region is obtained, the temperature distribution on the whole square fin can also be determined from Eq. (18). However, it should be noted that the average heat transfer coefficient on each sub-fin region is the approximate value. Thus the temperature distribution on the whole square fin is also an approximate contour for various V_{air} and S values. Figs. 8 and 9 show the distributions of the calculated temperature on the whole square fin for $S = 0.005$ m and various air speeds. The distributions of the calculated temperature on the fin for $S = 0.015$ m and various air speeds are shown in Figs. 10 and 11. It can be observed from Figs. 8–11 that, due to the poor thermal conductivity of the stainless fin, there is a considerable temperature drop between the tube wall and the edge of the square fin especially on the downstream region. The fin temperature distributions obviously depart from the ideal isothermal situation and the fin temperature decreases more rapidly away from the circular center when the V_{air} value increases. Due to the above phenomenon, the fin efficiency decreases with increasing the frontal air speed or the Reynolds number.

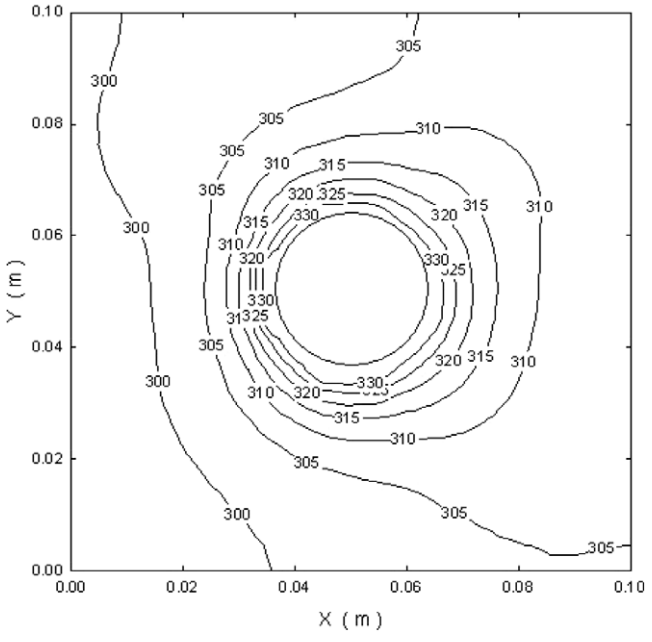

Fig. 8. Distribution of the calculated fin temperature for $S = 0.005$ m and $V_{air} = 1$ m/s.

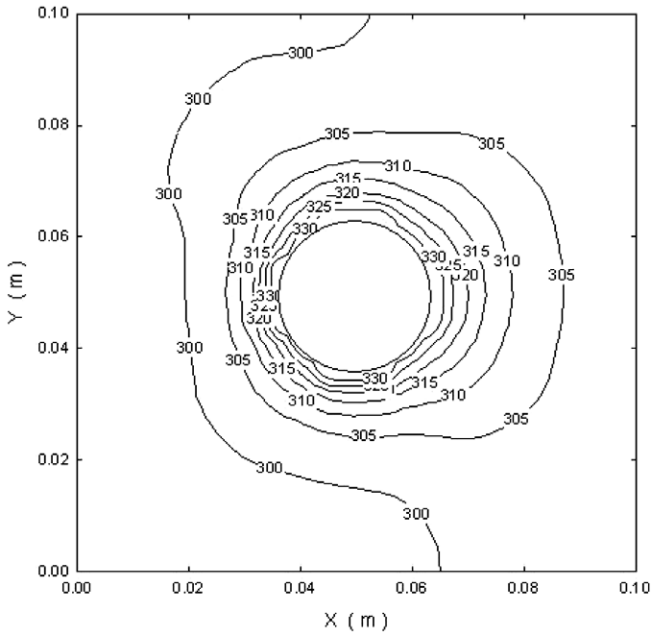

Fig. 9. Distribution of the calculated fin temperature for $S = 0.005$ m and $V_{air} = 3$ m/s.

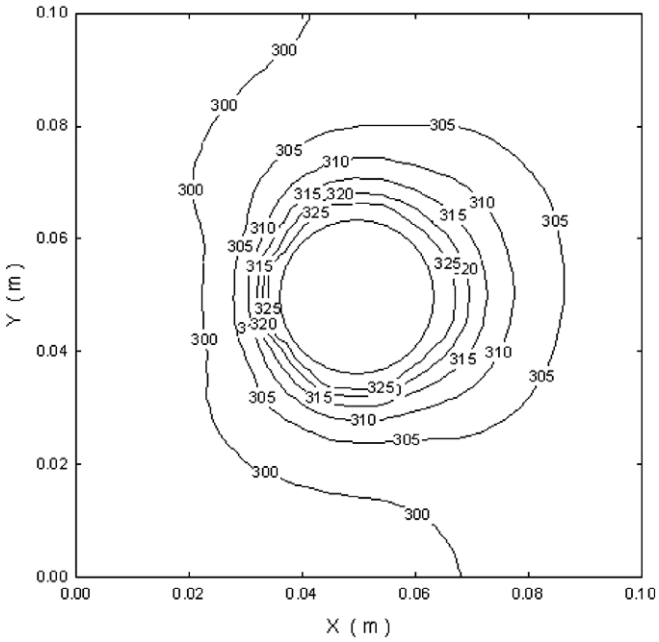

Fig. 11. Distribution of the calculated fin temperature for $S = 0.015$ m and $V_{air} = 3$ m/s.

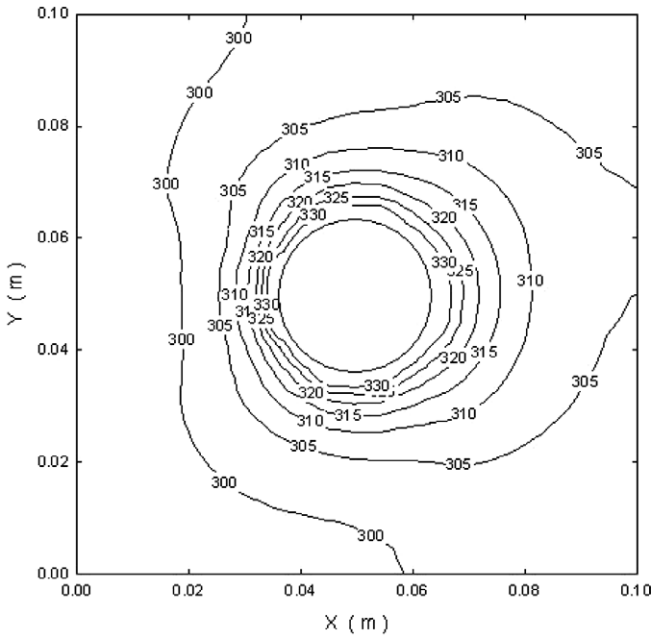

Fig. 10. Distribution of the calculated fin temperature for $S = 0.015$ m and $V_{air} = 1$ m/s.

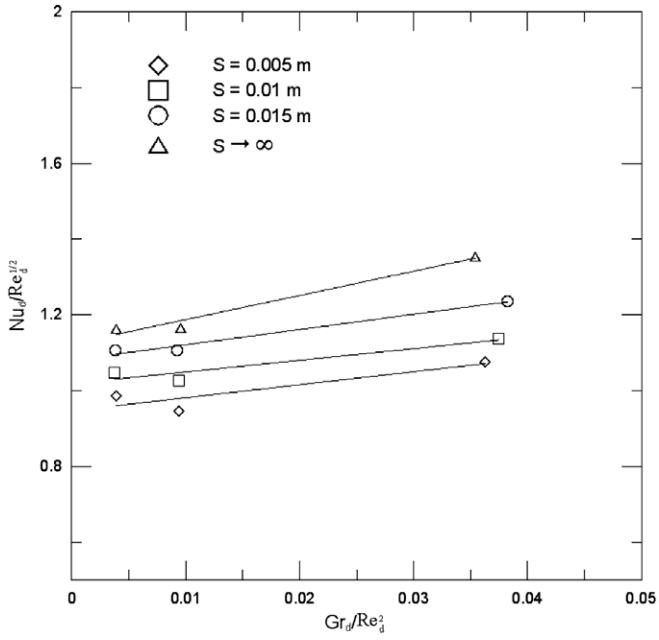

Fig. 12. Variation of $Nu_d/Re_d^{1/2}$ with Gr_d/Re_d^2.

Figs. 12 and 13 respectively show the effect of Gr_d/Re_d^2 on $Nu_d/Re_d^{1/2}$ and the fin efficiency η_f. The smoothing curves can be applied to match the data points of $Nu_d/Re_d^{1/2} - Gr_d/Re_d^2$ and $\eta_f - Gr_d/Re_d^2$. The correlations of $Nu_d/Re_d^{1/2} - Gr_d/Re_d^2$ and $\eta_f - Gr_d/Re_d^2$ can be obtained using the least-square fitting method of experimental data and are expressed as

$$\eta_f = \begin{cases} 0.115 + 10.084 \times GR_d - 564.689 \times GR_d^2 \\ \quad +13830.830 \times GR_d^3 \quad \text{for } S = 0.005 \text{ m} \\ 0.117 + 7.940 \times GR_d - 370.804 \times GR_d^2 \\ \quad +7468.036 \times GR_d^3 \quad \text{for } S = 0.01 \text{ m} \\ 0.123 + 4.067 \times GR_d - 94.409 \times GR_d^2 \\ \quad +654.805 \times GR_d^3 \quad \text{for } S = 0.015 \text{ m} \\ 0.112 + 4.320 \times GR_d - 105.092 \times GR_d^2 \\ \quad +901.626 \times GR_d^3 \quad \text{for } S \to \infty \end{cases} \tag{34}$$

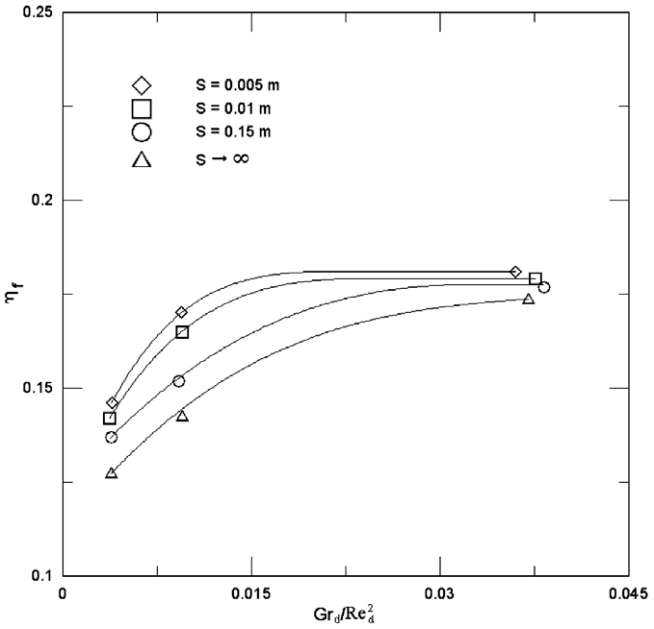

Fig. 13. Variation of η_f with Gr_d/Re_d^2.

and

$$Nu_d/Re_d^{1/2} = \begin{cases} 0.947 + 3.435 \times GR_d & \text{for } S = 0.005 \text{ m} \\ 1.018 + 3.073 \times GR_d & \text{for } S = 0.01 \text{ m} \\ 1.080 + 4.090 \times GR_d & \text{for } S = 0.015 \text{ m} \\ 1.123 + 6.404 \times GR_d & \text{for } S \to \infty \end{cases} \tag{35}$$

where Gr_d is the Grashof number, Re_d is the Reynolds number. The parameter GR_d is defined as $GR_d = Gr_d/Re_d^2$. The Nusselt number Nu_d is defined as

$$Nu_d = \frac{\bar{h} d_o}{k_{air}} \tag{36}$$

In Eq. (36), k_{air} denotes the thermal conductivity of the air.

Table 3 shows variations of $Nu_d/Re_d^{1/2}$, Gr_d/Re_d^2 and Re_d with various S and V_{air} values. It can be found from Table 3 that the Re_d value ranges about from 1500 to 4600, and the Gr_d/Re_d^2 value is less than 0.04 for various V_{air} and S values. Thus the airflow in the present problem is laminar for $V_{air} \leqq 3$ m/s and various S values. However, the tube sheds eddies, which wash over the fin surface and provide mixing of the flow. Lloyd and Sparrow [16] applied the local similarity method to investigate the effect of natural convection for combined natural and forced convection from a hot isothermal vertical plate. Their numerical results [2] showed that the effect of natural convection can be negligible for $(Gr_d/Re_d^2)(L/d_0) < 0.08$. On the other hand, the effect of natural convection will gradually become significant for $Gr_d/Re_d^2 > 0.08 d_0/L = 0.0218$ in the present problem. This implies that the effect of natural convection cannot be negligible for $V_{air} \leqq 1$ m/s and $S \geqq 0.005\,m$. Furthermore, it can also be found from Tables 1 and 2 that the measured fin temperatures on the top fin region, T_2^{mea} and T_3^{mea}, are higher than those on the bottom fin region, T_7^{mea} and T_8^{mea}. This result displays that the effect of natural convection in the present problem can need to be taken into consideration for $V_{air} = 1$ m/s and $S \geqq 0.005$ m especially on the downstream fin region, and the effect of natural convection decreases with increasing the V_{air} value.

Table 3
Variations of Gr_d/Re_d^2, $Nu_d/Re_d^{1/2}$ and Re_d with various S and V_{air} values

		Gr_d/Re_d^2	$Nu_s/Re_d^{1/2}$	Re_d
$S = 0.005$ m	$V_{air} = 1$ m/s	0.03625	1.0765	1520.6016
	$V_{air} = 2$ m/s	0.00937	0.9462	3035.2446
	$V_{air} = 3$ m/s	0.00389	0.9868	4589.1051
$S = 0.01$ m	$V_{air} = 1$ m/s	0.03748	1.1371	1515.0223
	$V_{air} = 2$ m/s	0.00942	1.0251	3042.065
	$V_{air} = 3$ m/s	0.00373	1.048	4619.1311
$S = 0.015$ m	$V_{air} = 1$ m/s	0.03821	1.2362	1518.4509
	$V_{air} = 2$ m/s	0.00921	1.1052	3029.1896
	$V_{air} = 3$ m/s	0.00378	1.1058	4619.3828
$S \to \infty$	$V_{air} = 1$ m/s	0.03544	1.3531	1521.4636
	$V_{air} = 2$ m/s	0.00953	1.1661	3019.2562
	$V_{air} = 3$ m/s	0.00387	1.1624	4599.5914

6. Conclusions

The present study proposes a numerical inverse scheme involving the finite difference method in conjunction with the least-squares method and experimental fin temperatures at eight measurement locations to estimate the heat transfer coefficients on eight sub-fin regions, average heat transfer coefficient on the whole square fin $\bar{h}$ and fin efficiency η_f for various T_o, T_∞, V_{air} and S values. The estimated results show that there is a considerable temperature drop between the tube wall and the edge of the square fin especially on the downstream region. The fin temperature distributions depart from the ideal isothermal situation and the fin temperature decreases more rapidly away from the circular center with increasing the fin spacing and air speed. The average heat transfer coefficients are very low on the downstream fin region behind the circular tube. The ratio of the average heat transfer coefficient on the front fin region to that on the wake fin region can be up to 10 times under the given conditions of V_{air}, T_o and T_∞. The $\bar{h}$ value increases with increasing the S and V_{air} values. However, the η_f value decreases with increasing the V_{air} and S values. The present estimates also show that the $\bar{h}$ and η_f values respectively approach their corresponding asymptotical values obtained from a single fin as $S \to \infty$. On the other hand, the present estimated values of $\bar{h}$ can be obtained over a reasonably wide range of fin spacings.

Acknowledgements

The authors gratefully acknowledge the financial support provided by the National Science Council of the Republic of China under Grant No. NSC 92–2622–E006–146.

References

[1] R.L. Webb, Principles of Enhanced Heat Transfer, Wiley, New York, 1994, pp. 125–153.

[2] Y.A. Çengel, Heat Transfer – A practical approach, second ed., McGraw-Hill, New York, 2004, pp. 486–488.

[3] M.N. Özisik, Heat Conduction, second ed., Wiley, New York, 1993 (Chapter 14).

[4] K. Kurpisz, A.J. Nowak, Inverse Thermal Problems, Computational Mechanics Publications, Southampton, UK, 1995.

[5] T.V. Jones, C.M.B. Russell, Efficiency of rectangular fins, in: ASME/AIChE National Heat Transfer Conference, Orlando, Florida, 1980, pp. 27–30.

[6] F.E.M. Saboya, E.M. Sparrow, Local and average heat transfer coefficients for one-row plate fin and tube heat exchanger configurations, ASME J. Heat Transfer 96 (1974) 265–272.

[7] E.C. Rosman, P. Carajilescov, F.E.M. Saboya, Performance of one- and two-row tube and plate fin heat exchangers, ASME J. Heat Transfer 106 (1984) 627–632.

[8] H. Ay, J.Y. Jang, J.N. Yeh, Local heat transfer measurements of plate finned-tube heat exchangers by infrared thermography, Int. J. Heat Mass Transfer 45 (2002) 4069–4078.

[9] C.H. Huang, I.C. Yuan, H. Ay, A three-dimensional inverse problem in imaging the local heat transfer coefficients for plate finned-tube heat exchangers, Int. J. Heat Mass Transfer 46 (2003) 3629–3638.

[10] H.T. Chen, J.P. Song, Y.T. Wang, Prediction of heat transfer coefficient on the fin inside one-tube plate finned-tube heat exchangers, Int. J. Heat Mass Transfer 48 (2005) 2697–2707.

[11] H.T. Chen, J.C. Chou, Investigation of natural-convection heat transfer coefficient on the fin inside one-tube plate finned-tube heat exchangers, Int. J. Heat Mass Transfer 49 (2006) 3034–3044.

[12] M.S. Mon, U. Gross, Numerical study of fin-spacing effects in annular-finned tube heat exchangers, Int. J. Heat Mass Transfer 47 (2004) 1953–1964.

[13] A. Bejan, Heat Transfer, John Wiley & Sons, Inc., New York, 1993, pp. 53–62.

[14] H.T. Chen, J.T. Liou, Optimum dimensions of the continuous plate fin for various tube arrays, Numer. Heat Transfer A 34 (1998) 151–167.

[15] V.S. Arpaci, S.H. Kao, A. Selamet, Introduction to Heat Transfer, Prentice-Hall, NJ, 1999, pp. 202–205.

[16] J.R. Lloyd, E.M. Sparrow, Combined forced and free convection flow on a vertical surface, Int. J. Heat Mass Transfer 13 (1970) 434–438.